Ultrafast internal conversion pathway and mechanism in 2-(2′-hydroxyphenyl)benzothiazole: a case study for excited-state intramolecular proton transfer systems

Mario Barbatti,*[a] Adélia J. A. Aquino,[a] Hans Lischka,*[a] Christian Schriever,[b] Stefan Lochbrunner†[b] and Eberhard Riedle*[b]

Received 15th August 2008, Accepted 26th November 2008
First published as an Advance Article on the web 13th January 2009
DOI: 10.1039/b814255f

We study the ultrafast electronic relaxation of the proton transfer compound 2-(2′-hydroxyphenyl)benzothiazole (HBT) in a joint approach of femtosecond pump–probe experiments and dynamics simulations. The measurements show a lifetime of 2.6 ps for the isolated molecule in the gas phase in contrast to ~100 ps for cyclohexane solution. This unexpected decrease by a factor of 40 for the gas phase is explained by ultrafast internal conversion to the ground state promoted by an inter-ring torsional mode. The quantum chemical calculations based on multireference configuration interaction clearly demonstrate that a S_0/S_1 conical intersection at a 90° twisted structure exists and is responsible for the ultrafast decay. The reaction path leading from the keto form of HBT to this intersection is practically barrierless on the S_1 surface. The on-the-fly dynamics simulations using time-dependent density functional theory show that after electronic excitation to the S_1 state and after fast excited-state proton transfer (30–50 fs), HBT reaches the region of the S_1/S_0 crossing within about 500 fs, which will lead to the observed 2.6 ps deactivation to the ground state. After the internal conversion, HBT branches in two populations, one that rapidly closes the proton transfer cycle and another (*trans*-keto) that takes ~100 ps for that step.

Introduction

Molecules exhibiting intramolecular proton transfer in the electronically excited state (ESIPT) are intensively studied to gain insight into fundamental photophysical and photochemical processes and to explore their potential to applications *e.g.* as dyes and sunscreens.[1–8] Detailed experimental and theoretical investigations for cases such as HBT (2-(2′-hydroxyphenyl)-benzothiazole), 10-HBQ (10-hydroxybenzo[h]quinoline), and $BP(OH)_2$ ((2,2′-bipyridyl)-3,3′-diol) show that the photo-initiated proton transfer proceeds as a ballistic wavepacket motion on a timescale of less than 50 fs and involves skeletal deformations that modulate the donor–acceptor distance.[7,9–13] Although the ESIPT is very similar in all these molecules striking differences in the internal conversion (IC) rates are found. The IC times vary by almost four orders of magnitude from 150 fs for TINUVIN-P[14] to 0.86 ns for 2-(2′-hydroxyphenyl)-4-methylthiazole in methylcyclohexane.[15] The fluorescence spectra indicate that the energy gap between the ground and excited state varies only by a factor of 1.5 among the considered molecules and thus cannot account for such variations in the IC rate. For most investigated ESIPT molecules, the IC accelerates with increasing temperature[1,5,15] and a strong influence of the solvent has been observed.[1,9]

HBT (see Fig. 1) has served as a basic example for many ESIPT studies.[1,6,10,12,16,17] The proton transfer causes a substantial rearrangement in the electronic structure, which leads to a strong Stokes shift of about 9000 cm^{-1} in non-polar solvents.[10] Recently, we applied transient absorption experiments with 30 fs time resolution in combination with classical and wavepacket dynamics simulations to understand in detail how the proton transfer process takes place in HBT and in the related system 10-HBQ.[12] These investigations confirmed the ultrashort time scale (30–50 fs) of the ESIPT and gave a detailed picture of structural and mechanistic aspects of that process. The subsequent IC had not been the subject of those investigations.

In all these studies of HBT the molecule was considered as planar. The photoexcitation of HBT and the consequent biradical character connected with the thiazole and hydroxyl-phenyl rings due to the proton transfer could, however, trigger a torsional motion around the CC-inter-ring bond (Fig. 1) in the same way as it occurs upon the photoexcitation of systems like ethylene,[18] stilbene[19,20] or azobenzene.[21] This kind of motion plays a key role in photochemistry since it may lead to an avoided crossing or even to a conical intersection between the excited state and the ground state after twisting by 90° (see ref. 22–26), leading to an ultrafast IC rate in the second case. In fact, the importance of such torsions for the internal conversion process in ESIPT-triggered systems has been suggested previously based on spectroscopic

[a] *Institute for Theoretical Chemistry, University of Vienna, Waehringerstrasse 17, A-1090 Vienna, Austria. E-mail: mario.barbatti@univie.ac.at. E-mail: hans.lischka@univie.ac.at*
[b] *Fakultät für Physik – Ludwig-Maximilians-Universität (LMU), Oettingenstr. 67, D-80538 München, Germany. E-mail: eberhard.riedle@physik.uni-muenchen.de*
† [1]Present address: Institut für Physik, Universität Rostock, Universitätsplatz 3, D-18055 Rostock, Germany.

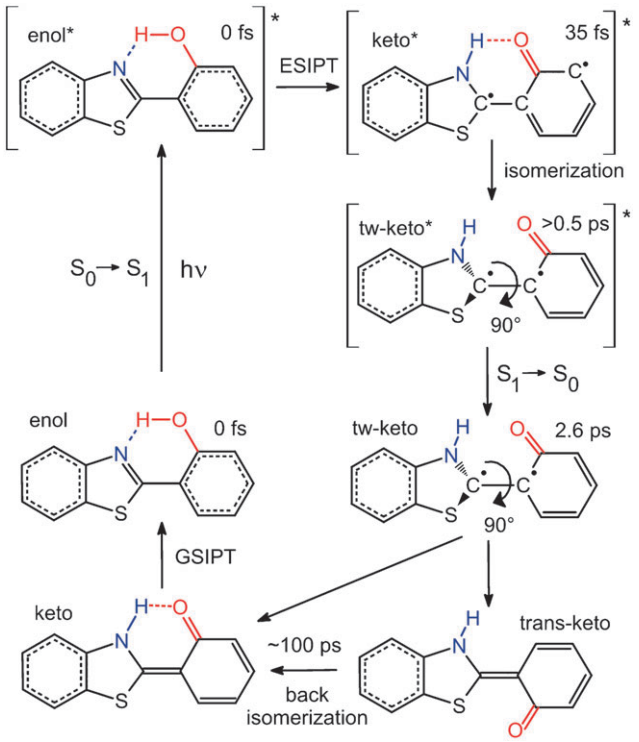

Fig. 1 Schematic representation of the internal conversion in HBT in the gas phase. After photo-excitation, excited state proton transfer (ESIPT) triggers the isomerization, which brings the system to a conical intersection. HBT returns to the ground state by internal conversion. The ground state relaxation, which includes the back proton transfer (GSIPT), completes the cycle. A long-lived population of *trans*-keto is also observed. The timings added to selected structures indicate their clock time starting with the absorption process of a photon in the enol form of HBT.

investigations.[1,27] Recent calculations on 2-(2′-hydroxyphenyl)-benzotriazole (TIN-H),[8] closely related to HBT and on 7-(2-pyridyl)indole[28] show that such a torsion actually may occur. Femtosecond experiments performed for the latter compound confirm this view.[29] However, the measured fluorescence spectra (and consequently the long excited-state life time) show that this is not the case for HBT in solution, at least not in the solvents that have been used so far.

Even though the ultrafast dynamics of the initial ESIPT seems to be very well understood, the large variation in the IC times mentioned above shows that the mechanism of this step, which follows the ESIPT, is very subtle and still awaits a thorough understanding. Therefore, we again join experimental and theoretical efforts in this work in order to study the dynamics of the IC process occurring in HBT and to investigate in particular the actual possibilities for ultrafast decay to the ground state along the lines discussed in the previous paragraph. In order to work out the effect of the torsional motion and separate it from environmental effects, the pump–probe experiments with 20-fs time-resolution have to be performed in the gas phase. Such very precise measurements with sufficient temporal resolution to resolve the relevant nuclear motion are extremely demanding and have not been performed on ESIPT systems before. The technical details of these measurements have already been reported.[30] It is the purpose of this work to present a first analysis of the spectroscopic results in combination with matching theoretical calculations. The quantum chemical calculations on electronically excited states are not less demanding because of the size of the HBT molecule and the occurrence of intersections between different energy surfaces. Moreover, it is our goal to simulate the dynamics of the IC process, which increases computational demands drastically. We want to show that this combination of state-of-the-art experimental and theoretical investigations reveals details of the photodynamical processes at a so far unprecedented level.

Computational details

Classical dynamics simulations were performed for HBT on the first singlet excited state (S_1) energy surface. Thirty trajectories were simulated up to a maximum of 500 fs with a time step of 1 fs. This relatively small number of trajectories has been chosen in view of the long simulation times and because in our investigations the focus was laid on the main mechanistic pathway, which does not require large samples to be statistically described. The velocity Verlet algorithm[31] was applied to solve Newton's equations of nuclear motion. The Born–Oppenheimer energies and gradients were obtained "on the fly" at each time step by means of the TD-DFT approach[32–34] using the B3-LYP functional.[35] In previous investigations[6,8,12] it has been shown that the resolution-of-identity second-order approximate coupled-cluster (RI-CC2) method[36–38] is very well suited to provide benchmark results in order to assess eventual artifacts of the TD-DFT method. Comparisons for a series of ESIPT cases including HBT and HBQ[6,12] demonstrated that TD-DFT gives quite reliable results for the proton transfer process in the $\pi\pi^*$ state. The verification of the TD-DFT results is especially important for the on-the-fly dynamics technique used here where thousands of quantum chemical calculations have to be performed and computationally efficient methods such as TD-DFT are required. The question of the applicability of TD-DFT for the CC-inter-ring torsional motion will be discussed below. However, also in this case it was found by comparison with complete active space self-consistent field (CASSCF), multireference configuration interaction (MRCI) and RI-CC2 methods that TD-DFT gave acceptable results until the stage where the biradical character started to dominate. The SV(P) basis set[39] was applied for all atoms except the migrating hydrogen atom, to which the polarization functions of the full SVP basis set were added. Throughout this work, this basis set choice will be referred as SV(P)*. Test calculations comparing the full SVP, the SV(P) and the SV(P)* basis sets had shown that the p functions on the migrating hydrogen are important. Furthermore, comparison of results obtained with the SVP and TZVP basis sets[6] showed very good agreement in vertical and adiabatic excitation energies and optimized geometries, meaning that the SV(P)* basis is an efficient candidate to be used in the extended on-the-fly dynamics calculations. The initial conditions for each trajectory were generated by sampling the coordinates and momenta so as to reproduce the ground-vibrational quantum harmonic distribution of the electronic ground state by means

of a Wigner distribution. The ground-state geometries and velocities were used as initial conditions for the trajectories in the excited state. For more details see ref. 40.

The trajectory dephasing discussed below in the General Discussion was calculated in the following way. The S_1–S_0 transition energy as a function of time was collected from the trajectories. For each time interval i of 10 fs in the course of the dynamics the number n_i of trajectories with energy lying in the range $E_{av} \pm \Delta E$ was counted, where E_{av} is the average transition energy in the interval i and ΔE was set to 0.2 eV. The number n_i was normalized by the total number of points in the interval. Finally, the dephasing function $\Phi(t)$ is defined by these values n_i normalized by their average value between 100 and 200 fs. During this period, the width only fluctuates around a constant value.

Additional calculations were performed for stationary points and cuts on the potential energy surface at the RI-CC2, MRCI, and CASSCF methods. These calculations aimed at the examination of the formation of the biradical character due to the inter-ring torsion. An appropriate wavefunction describing the quasi-degeneracy (non-dynamical electron correlation) of the biradical system formed is a CAS(2,2) with two electrons in two orbitals. Therefore, in the first place CASSCF(2,2) calculations were performed with state-averaging over the ground state and the first singlet excited state (SA-2). In order to take into account dynamical electron correlation effects, MRCI calculations with a CAS(2,2) reference space and with inclusion of all single and double excitations (MR-CISD) into the virtual orbital space were carried out based on the SA-2-CASSCF(2,2) molecular orbitals. The core orbitals were kept frozen in the MRCI procedure. Higher-order excitation effects were taken into account by means of the Pople correction (+Q).[41–43] The main purpose of these calculations was the demonstration of the existence of the S_1/S_0 crossing for which the use of true multireference methods is crucial. The 3-21G and a mixed 6-31G(d,p)/6-31G basis set[44,45] were selected for the CASSCF calculations. In the mixed basis, denoted 6-31G-mix, the 6-31G(d,p) basis was used except for the carbon atoms of the benzene ring of the benzothiazole system and the hydrogen atoms not involved in the hydrogen bond. For these latter atoms the 6-31G basis was applied. In view of the size of HBT the MR-CISD calculations were performed only with the smaller basis set. It has also been shown previously by comparison between 3-21G and 6-31G* basis sets for protonated Schiff bases[46] that the 3-21G basis can describe torsional potentials leading to biradical character quite well. The SV(P)* was used in the RI-CC2 calculations. However, it should be mentioned that this method, because of its single-reference character, will also not be applicable for the proper description of the biradical nature of the inter-ring torsion in HBT.

Stationary points and minima on the crossing seam were obtained at the SA-2-CASSCF/6-31G-mix level with the routines for analytical energy gradients and nonadiabatic coupling vectors[43,47–50] as implemented in the COLUMBUS program package.[51–53] COLUMBUS was also used for the MRCI calculations. The excited-state dynamics simulations were performed with the NEWTON-X program[40,54] using TD-DFT energy gradients[55] provided by the TURBOMOLE program package.[56] All additional TD-DFT and RI-CC2 calculations were performed with the TURBOMOLE program package as well.

Experimental details

The transient absorption of HBT in the gas phase and in cyclohexane solution is measured with a pump–probe spectrometer based on two noncollinearly phase matched optical parametric amplifiers (NOPAs). The spectrometer is able to detect changes in the optical density as small as 10^{-6}.[30] In brief, two NOPAs[57] are pumped by a regenerative Ti:sapphire amplifier system (CPA 2001; Clark-MXR, Inc.). Chirped sum frequency mixing of the output of one NOPA with a fraction of the Ti:sapphire beam results in ultraviolet (UV) pump pulses at 325 nm.[58] The output of the second NOPA serves as probe beam. To obtain a sufficient sensitivity for low density gas phase samples a collinear focusing geometry with a long Rayleigh range and an interaction length of 50 mm is applied. For the gas phase experiments, HBT is heated to about 125 °C in an evacuated cell to increase the vapor pressure. For measurements on HBT in cyclohexane a 3×10^{-3} M solution is pumped through a cuvette with an optical path length of 120 μm. This allows us, by just exchanging the cells, to compare directly the molecular dynamics in the gas phase and in solution.

Results and discussion

Experimental results

To understand the influence of the environment on the IC of HBT, we compare the photoinduced dynamics of the solvated and the isolated molecule. The steady state absorption and emission spectra in the gas phase are blue shifted by about 800 cm^{-1} and 500 cm^{-1} relative to the spectra in cyclohexane (not shown). The 325 nm pump pulses promote HBT both in solution and in the gas phase into the S_1 state. The induced transmission change measured at 560 nm is shown in Fig. 2a for both cases. The initial transmission rise is due to the emission from the keto form in the electronically excited state, populated by the ultrafast ESIPT.[10] In solution, only wavepacket dynamics but no change of the average signal is observed on the picosecond time scale and the stimulated emission decays with a time constant of ~100 ps in good agreement with previous reports.[1,27] It reflects the deactivation to the electronic ground state. The weak oscillatory feature due to 108 cm^{-1} wavepacket dynamics is observed in good agreement with values reported previously[10] (see Fig. 2c). It results from the coherent excitation of an in-plane bending vibration promoting the ESIPT.

The transient absorption of HBT in the gas phase also exhibits an initial transmission rise due to stimulated emission from the keto form (see Fig. 2a). The emission decays quite rapidly and vanishes within 5 ps. Contrary to the solution data a large, but strongly damped, low-frequency oscillation is found in addition. A model function with a fast and a slow decay is fitted to the data giving time constants of 2.6 ps and

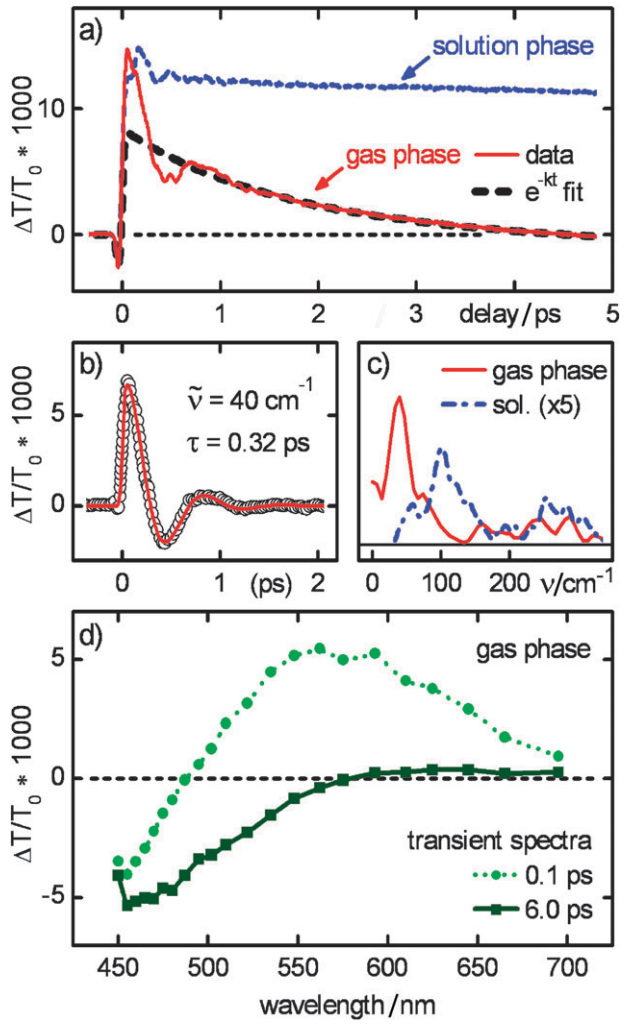

Fig. 2 (a) Time-resolved transmission change of HBT in cyclohexane (dotted) and in the gas phase (solid) at 560 nm after excitation at 325 nm. An exponential fit (dashed) to the gas phase data reveals an IC time of 2.6 ps. (b) Residuum (circles) of the exponential fit modeled with a damped cosine function (solid). (c) Fourier transformations of the gas phase (solid) and solution phase (dash dotted, scaled by a factor of 5) residuum. (d) Transient spectra at a delay time of 0.1 ps and 6 ps reconstructed from time traces measured at different probe wavelengths.

100 ps. The fast time describes the emission decay and characterizes the IC rate. Obviously, the IC in the gas phase is about 40 times faster than in the cyclohexane solution. After the emission decay a small residual absorption (negative-going signal) remains which can be seen from the crossing of the experimental trace with the zero line at 4.5 ps. This absorption disappears on a time scale of 100 ps according to the fit. We tentatively assign it to a *trans*-keto tautomer in the electronic ground state. This tautomer was observed after photoexcitation of HBT dissolved in chloroform and has a broad absorption band around 460 nm.[59] Measurements at probe wavelengths between 450 and 690 nm were combined to reconstruct the transient spectrum at 0.1 and 6.0 ps (see Fig. 2d). The initial stimulated emission signal around 560 nm and the excited state absorption starting in the blue is changed within this time delay to a purely absorptive signal increasing toward 450 nm. The spectral shape suggests that we see the above mentioned 460 nm band and supports the proposed assignment to the *trans*-keto tautomer.

Fig. 2b displays the residuum of the gas phase data after subtracting the exponential contributions, which exhibits a pronounced and strongly damped oscillatory behavior. Fitting an exponentially damped cosine function to the residuum reveals a frequency of 40 cm^{-1} and a damping time of 0.32 ps in agreement with the residuum's Fourier transformation (see Fig. 2c).

Discussion of the experimental results

The femtosecond experiments find for HBT an acceleration of the IC in the gas phase by a factor of 40 compared to the cyclohexane solution. Also for *o*-hydroxybenzaldehyde (OHBA) a 13-times-faster IC was observed in the gas phase compared to a cyclohexane solution.[9,60] This indicates that the faster IC in the gas phase may be a wide spread feature of ESIPT compounds. Viscosity is a rate limiting factor that is only present in solution. A reduction of the IC rate with increasing viscosity has already been observed for several ESIPT compounds like HBT,[1,27,61] 1′-hydroxy-2′-acetonaphthone,[5] and (1-hydroxy-2-naphthyl)-s-triazine.[62] This was interpreted as a strong indication that a *cis–trans* isomerization promotes the IC.[1,5,27,61,62] In our femtosecond experiments this motion is for the first time directly observed. They show that after the ESIPT a wavepacket motion along the torsional coordinate exists leading to the region of the PES where a conical intersection should be located. This strongly supports the results of the trajectory calculations (see below), which find that the torsional mode is dominant on the picosecond scale and that a conical intersection does indeed exist near the 90° twisted structure.

As the wavepacket leaves the planar keto conformation, the experimentally observed transient signal shows a mono-exponential decay with a time constant of 2.6 ps. This decay corresponds well to the predictions from non-adiabatic dynamics focusing on torsional oscillation with dephasing. Although more-complex kinetics could be expected from the oriented multidimensional dynamics, the mono-exponential function fits the data very well and therefore a more-complex parametrization is not justified. The interpretation of the dynamics is, however, not based on this particular fit function and temporal behavior.

At the twisted conformation a branching can occur to the *cis*-keto or the *trans*-keto ground state (Fig. 1). The latter one cannot undergo fast proton back-transfer and is long lived.[59] This is in line with our observation of a 100 ps transient absorption which can be assigned to the *trans*-keto tautomer.

The large difference between the gas and solution phase can be rationalized as follows. In the gas phase the molecule propagates in a ballistic way directly to the region of very efficient IC. This motion is associated with a large-amplitude twisting of the entire molecular skeleton. In solution, it is strongly damped by friction due to interaction with the solvent molecules. Thereby the ballistic motion is stopped and the torsion evolves in a statistical fashion, similar to a Brownian motion.

Torsional coordinate and conical intersection

The discussion above shows that the torsional motion around the inter-ring bond between the benzthiazole and hydroxyphenyl moieties plays a crucial role. Previous TDDFT/B3LYP calculations have shown[6] that for the keto form in the S_1 state one imaginary vibrational frequency exists, which was characterized by the inter-ring torsion (note a corresponding misprint in Table 10 of ref. 6 where the value in brackets for the ππ*(keto) form should be one instead of zero). Therefore, extensive investigations have been performed using several quantum chemical methods in order to establish the reliability of the obtained results. Such tests are especially important for the verification of the TD-DFT method for several reasons: first, this method may predict a wrong charge distribution for biradicaloid states, which would result in a wrong description of the potential energy along the torsional coordinate;[63] second, during the excited state relaxation the system may reach geometries with strong multireference character, which obviously cannot be adequately described with single-reference methods and third, because of general problems with respect to the proper description of charge-transfer states.[64] Nevertheless, the computational efficiency and the availability of analytical gradients make TD-DFT one of the few methods available to perform on-the-fly excited-state dynamics simulations for systems as large as HBT and for simulation times as long as 500 fs. In view of these potential drawbacks, we have performed comparisons between relevant cuts on the HBT potential energy surfaces calculated with TD-DFT and other single- and multireference methods, in order to validate the theoretical level used in the dynamics calculations.

Four different theoretical methods have been employed for the characterization of the potential energy of HBT along the torsional coordinate. The resulting curves are displayed in Fig. 3a and b, and characteristic points are collected in Table 1. For each fixed torsional angle θ the remaining coordinates were optimized for the S_1 state. The Figure shows, for all employed methods, a similar flat but effectively barrierless S_1 curve. Due to the single-reference character of the TD-DFT and RI-CC2 methods, it was not possible to compute the energies for torsional angles larger than 70° and 60°, respectively. As will be discussed below, this is also true for the dynamics calculations. For both methods, however, the same trend of drastically reducing the S_1–S_0 energy gap at large torsions is observed. In Fig. 3c the torsional dependence of the Einstein coefficient $B(\theta)$ for stimulated emission[65] is shown. It is calculated from the transition dipole moment $\mu_{10}(\theta)$ (CASSCF values) as

$$B(\theta) = \frac{1}{6\varepsilon_0\hbar^2}|\mu_{10}(\theta)|^2 \qquad (1)$$

where ε_0 is the vacuum permittivity and $\hbar$ is Planck's constant divided by 2π. This torsional behavior will be discussed below.

The vertical excitation energies computed at the CASSCF and MRCI+Q levels are too high by 1.8 and 1.3 eV, respectively. This is a typical behavior of these methods already found for smaller molecules such as ethylene and butadiene[66,67] and extensive MRCI calculations have to be

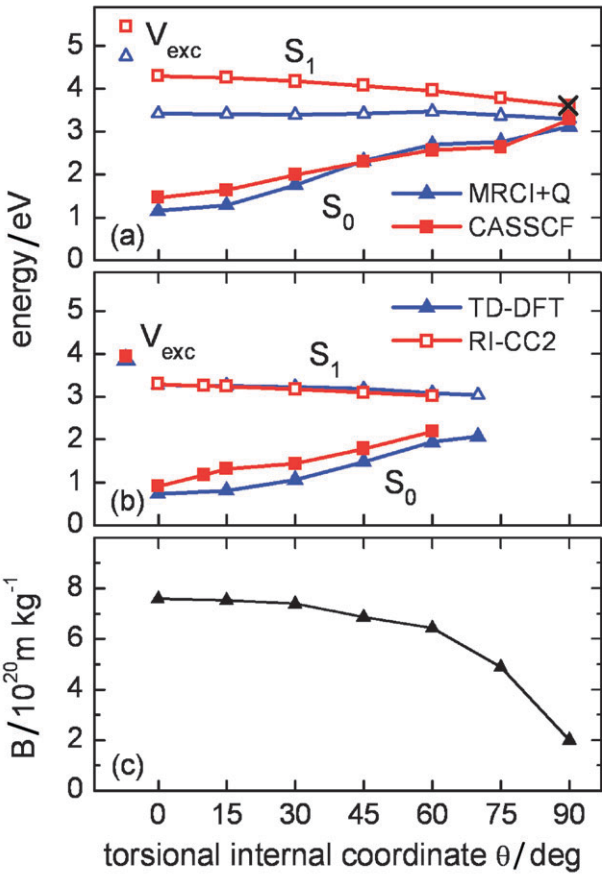

Fig. 3 Potential energy curves along the relaxed torsional coordinate for HBT. (a) SA-2-CASSCF(2,2)/6-31G-mix and MR-CISD+Q/SA-2-CASSCF(2,2)/3-21G. (b) TD-DFT(B3-LYP)/SV(P)* and RI-CC2/SV(P)*. (c) Einstein coefficient B for stimulated emission obtained at the SA-2-CASSCF(2,2)/3-21G level. The cross in (a) indicates the energy of the minimum on the crossing seam.

performed (see *e.g.* ref. 66, 68) which are out of reach for molecules of the size of HBT. The performance of MRCI+Q improves considerably for the minimum-to-minimum and fluorescence transitions. For the conical intersection it provides the correct multireference character and is generally applicable in contrast to the TDDFT and RI-CC2 methods. Therefore, we use these methods especially for the direct proof of the existence of a conical intersection at a strongly twisted HBT structure.

The complete torsional CASSCF and MRCI+Q curves until 90° are displayed in Fig. 3a. The MRCI+Q curves have been computed using optimized CASSCF/3-21G geometries. In the last point (90°), the restricted optimization at CASSCF level resulted in almost degeneracy between S_1 and S_0 (ΔE = 0.3 eV) indicating a conical intersection. The CASSCF and the MRCI+Q results using the CASSCF geometries showed that the effect of inclusion of dynamic electron correlation basically leads to a vertical shift in all points, producing almost parallel torsional curves in the excited state. Note that the reaction path was calculated in terms of natural internal coordinates[69] where the natural torsional internal coordinate is defined as the average of the four dihedral angles NCCC

Table 1 Energies of optimized structures and conical intersection of HBT

		Energy/eV				
Geometry	*State*	CASSCF[a]	MRCI + Q[b]	TD-DFT	RI-CC2	Exp[e]
Min S_0 (enol)	S_0	0.00	0.00	0.00	0.00	0.00
	S_1	5.46	4.76	3.86	3.94	3.68
Min S_1 (keto)	S_0	1.46	1.15	0.73	0.92	—
	S_1	4.29	3.42	3.28	3.30	—
Fluorescence	$S_1 \rightarrow S_0$	2.83	2.27	2.55	2.38	2.29
Conical intersection	S_1/S_0	3.61/3.61	3.11/3.30	~2.6[c]	~2.6[d]	—

[a] SA-2-CASSCF(2,2)/6-31G-mix. [b] MRCI + Q/SA-2-CASSCF(2,2)/3-21G//SA-2-CASSCF(2,2)/3-21G. [c] Average between the energies of the S_1 and S_0 states at 70°. [d] Average between the energies of the S_1 and S_0 states at 60°. [e] Experimental data from ref. 74.

(*cis*), NCCC (*trans*), SCCC (*cis*), and SCCC (*trans*). Although this average coordinate is kept constant during the optimization procedure, each individual dihedral angle can change, as can be seen from the values of the NCCC (*cis*) and SCCC (*cis*) dihedral angles in Fig. 4c. This means that the twisted structure also shows some degree of pyramidalization at the bridge carbon of the thiazole ring after the optimization. Along the reaction pathway, the migrating hydrogen is strongly displaced out of the thiazole ring in the direction of the oxygen atom.

The search for the minimum on the crossing seam reveals a conical intersection very close to the 90° twisted structure. Its CASSCF energy is indicated by a cross in Fig. 3a. The structure of this conical intersection is shown in Fig. 4c. Fig. 4 also shows the geometries optimized at the CASSCF level of the ground-state (enol, Fig. 4a) and the excited-state (keto, Fig. 4b). Geometries optimized at TD-DFT and RI-CC2 levels using triple-ζ quality basis set have been reported previously.[6] The change in the geometrical parameters indicates that the excited state relaxation affects mostly the hydroxyphenyl and the thiazole rings. In the twisted geometry, the biradical structure localizes across the CC bridge in analogy to what also happens in TIN-H.[8]

Excited-state dynamics simulations

The barrierless path connecting the Franck–Condon region to the S_1/S_0 conical intersection is a good indication for the possibility for HBT to display an ultrafast decay in the gas phase. The flatness of the excited state potential energy curve, however, could imply that HBT will not preferentially follow the torsional motion or if it does, it might take a relatively long time. This question can be addressed directly by performing excited-state dynamics calculations. As already mentioned above, thirty trajectories were computed at the TD-DFT(B3-LYP)/SV(P)* level for a maximum of 500 fs. Most of trajectories (25) run at least 400 fs, but only six of them completed 500 fs without finishing due to an error in the TD-DFT section of the calculation. This error was a consequence of the fact that the multireference character becomes important between 400 fs and 500 fs and it was not possible to continue the simulation using TD-DFT. Despite the fact that the simulations could not be completed at the TD-DFT level, the current results still show quite conclusively some interesting features that can help to understand the IC of HBT in the gas phase.

Fig. 5 shows the excited-state potential energy as a function of time for one of the trajectories that completed 500 fs. The ground-state potential energy for the same geometries and the S_1–S_0 energy gap are shown as well. A quite similar general behavior is found for all trajectories. The fast oscillation in the potential energy corresponds to the hydrogen stretching motions. The dynamics starts in an approximately planar structure depending on the initial conditions and after 30 fs the proton transfer is observed. This first part of the dynamics has already been described in detail.[12] In the trajectory shown

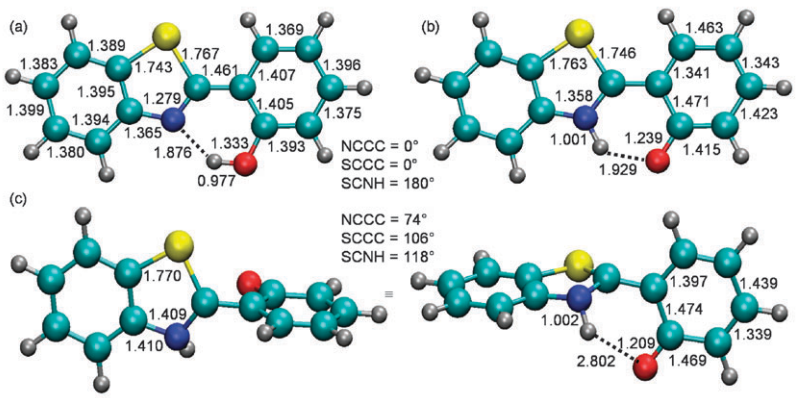

Fig. 4 (a) Ground state (enol), (b) planar excited state (keto), and (c) twisted excited state optimized geometries at the SA-2-CASSCF(2,2)/6-31G-mix level. In (b) and (c) the bond lengths are given only for those bonds that change more than 0.01 Å in comparison to the ground state structure (a). (c) shows two different views of the same structure. All bond lengths in Å.

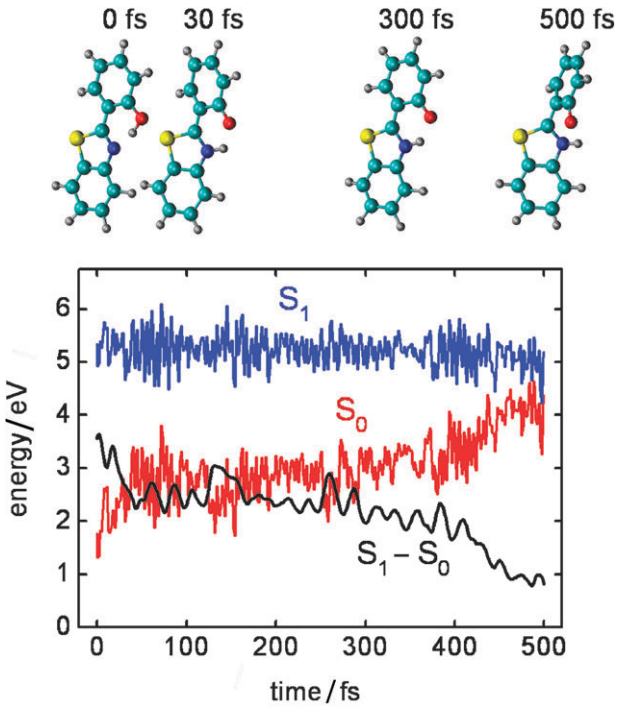

Fig. 5 S_1 and S_0 energies of HBT for a selected excited state trajectory. The energy difference between the two states is also plotted. Snapshots are given at 0 fs (Franck–Condon region), 30 fs (proton transfer), 300 fs (beginning of torsional motion), and 500 fs (end of simulation).

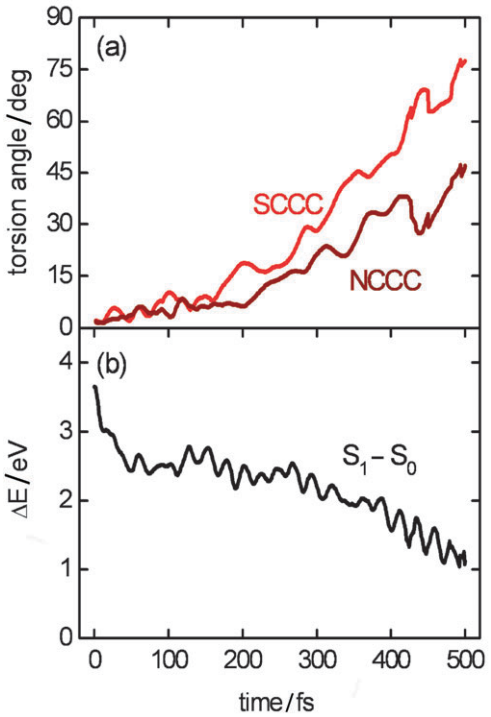

Fig. 6 Average over all trajectories of (a) the absolute value of the NCCC (*cis*) and SCCC (*cis*) dihedral angles and (b) of the S_1–S_0 energy gap, both as a function of time.

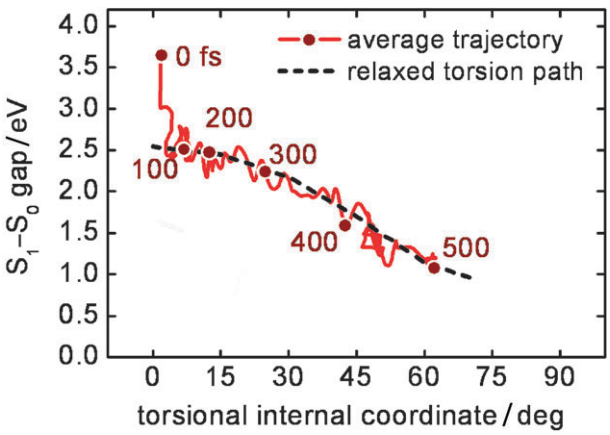

Fig. 7 S_1–S_0 energy gap as obtained from the average trajectory and from the relaxed torsional potential energy curves as a function of the torsional internal coordinate. The full circles and the numbers next to them indicate the time in femtoseconds.

in Fig. 5, HBT remains essentially planar after the proton transfer for about 250 fs until the torsional motion starts to become effective. At 500 fs, the S_1–S_0 energy gap is reduced to 0.8 eV. Along the trajectory, the migrating hydrogen atom is moved out of the thiazole ring plane, indicating that the NH···O hydrogen bond still persists. At 500 fs this hydrogen has a dihedral angle of 41° with the thiazole ring and its distance to the oxygen atom is 2.20 Å. The pyramidalization occurs simultaneously with the torsional motion, which is far from being rigid, as can be inferred from the values 62° and 84° of the NCCC (*cis*) and SCCC (*cis*) dihedral angles at 500 fs.

The analysis of the complete set of trajectories shows similar features. The average value of the S_1–S_0 energy gap is reduced from 3.6 eV to 1.1 eV between 0 fs and 500 fs (Fig. 6b). As mentioned above, the pyramidalization causes an asymmetry between the NCCC (*cis*) and SCCC (*cis*) dihedral angles, as shown in Fig. 6a. While the SCCC angle reaches 68° at 500 fs, the NCCC angle is only 36° at the same time.

The overall motion is simply following the torsional potential depicted in Fig. 3b. This can be seen by investigating the average S_1–S_0 energy gap not as a function of time, as in Fig. 6b, but as function of the natural torsional internal coordinate. The average S_1–S_0 energy gaps as obtained from the dynamics and from the potential energy curve are plotted in Fig. 7. This figure shows a fast decrease of the gap from 3.64 eV to around 2.5 eV taking place in less than 100 fs, while HBT is still essentially planar. This process corresponds to the ESIPT. After that, the energy gap just oscillates around the curve predicted by the torsional potential, moving to regions where the IC is more efficient.

General discussion

In the discussion of the experimental results it was shown that the temporal evolution of the transient absorption for HBT in gas phase is composed of an ultrafast exponential decay and a pronounced damped oscillation with sub-50 cm^{-1} frequency (Fig. 2a). There exist only two sub-100 cm^{-1} normal modes in HBT, the overall butterfly vibration and the overall torsion. Both cannot be excited by optical excitation and are not

associated with the ESIPT.[13] Which molecular distortion gives rise to the observed signal is now discussed in the light of the just-described dynamics calculations.

The fact that the dynamics leads toward the conical intersection explains the ultrafast IC. Even though the dynamics calculations do not reach the intersection for technical reasons, they come sufficiently close to it allowing the safe prediction that HBT will indeed reach if not the crossing itself, but at least regions of small energy gaps. The static CASSCF and MR-CI calculations discussed above prove the existence of the intersection. On the other hand, it is difficult to predict actual lifetimes from our trajectories. We want to note already at this point that the torsional motion should not be regarded as a simple one-dimensional process but that, on the contrary, several modes will be coupled. This will be, *e.g.* the inter-ring stretching mode but also the weak aforementioned NH···O hydrogen bond and the NCCC and SCCC torsional angles. Our experience obtained from the analysis of several cases such as substituted ethylenes,[25,70] adenine,[71] and adenine model substances[23,72] is that the molecular motion does not proceed directly to the conical intersection but requires certain vibrational adjustments until the switching to the ground state can occur. Thus, it is expected that the actual decay time is significantly longer than the time for the first approach into the region of the conical intersection. Unfortunately, concrete lifetimes cannot be given from the calculations because of the already-mentioned breakdown of the TDDFT approach in the neighborhood of the conical intersection.

The second point regards the initial low-frequency damped oscillation observed in the pump–probe experiment in the gas phase (see Fig. 2b). A comprehensive theoretical explanation would require the simulation of the pump–probe experiment, which is presently not feasible, most of all because of the premature breaking of the TD-DFT trajectories. Therefore, the discussion will be limited to modulations of the intensity of the stimulated emission in the course of the torsional mode as a possible origin for the experimentally observed oscillations. The combination of three effects seems to be responsible for changes in the intensity of the stimulated emission along the torsional mode. The first one is the reduction of the Einstein coefficient B with the torsional angle displayed in Fig. 3c. This factor alone cannot explain the signal modulation because first the reduction in B is not sufficiently pronounced and second significant reductions in B are only observed at torsional angles above 60°, which are reached only after about 450 fs whereas the oscillatory mode analyzed in Fig. 2 shows the first minimum already at about 430 fs. Fig. 8 illustrates this situation by comparison of the experimental $\Delta T/T_0$ signal divided by the exponential component with the time evolution of the normalized Einstein coefficient B in the time range that is relevant for the torsional mode.

The second effect contributing to the decrease in the emission intensity consists in an increasing dephasing of the trajectories along the torsional motion, which also leads to a reduction of the transmission signal. The trajectory dephasing (*i.e.* the energy spreading) was obtained as explained in the Computational Details. The evolution of the dephasing $\Phi(t)$ is plotted in Fig. 8. Small values of $\Phi(t)$ imply a wider

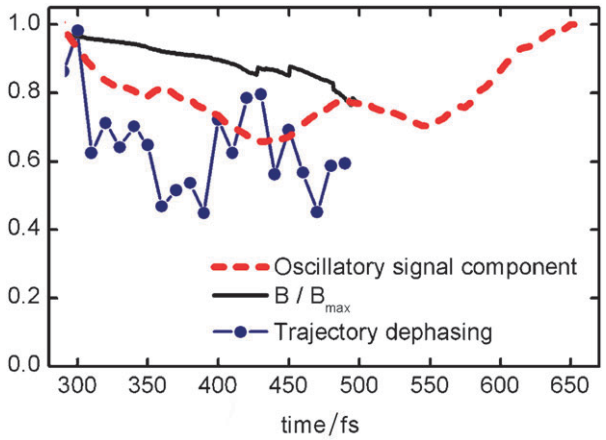

Fig. 8 Oscillatory signal component ($\Delta T/T_0$ divided by exponential component), average Einstein coefficient B/B_{max}, and trajectory dephasing $\Phi(t)$. All quantities are given as a function of time.

distribution of S_1/S_0 energy gaps and consequently a reduction of the stimulated emission for a given transition energy. The dephasing shows an early decrease with increasing torsion already in its initial stage and also displays a substructure similar to the one found in the experiment.

The third effect contributing to the signal reduction is the coupling of the torsion with the other vibrational modes and the consequent flow of energy into these modes as it is described, *e.g.* in ref. 20 will quickly reduce the amplitude of the torsional oscillations.

Together, the oscillation of the Einstein coefficient, the trajectory dephasing, and the energy dissipation will result in a damped oscillation of the stimulated emission probability.

Finally, it is worth calling attention to the trapping of HBT in the region near the S_1 minimum. This is the main point for the very-efficient IC. Were HBT able to reach the conical intersection, but quickly moved into other regions of the potential energy surface, as occurs for example in pyridone,[73] we might not expect any ultrafast behavior. This variability in the dynamical behavior is a key feature that can explain the fact mentioned in the Introduction that IC rates may change almost four orders of magnitude, while the energy gaps change by less than a factor of 1.5.

After the decay to the ground state at the twisted structure, HBT population splits in two branches, keto and *trans*-keto. While the keto isomer quickly returns to the initial enol isomer by ground state internal proton transfer (GSIPT), the *trans*-keto isomer takes about 100 ps in order to isomerize into the keto structure and then initiate the GSIPT (see Fig. 1). Note that the back isomerization is possible because in gas phase HBT remains vibrationally hot after the internal conversion.

Conclusions and final remarks

From the combined theoretical and experimental investigations we gain a thorough understanding of the internal conversion processes following the excited-state intramolecular proton transfer in HBT. For a summary of the entire process cycle as determined by our investigations see Fig. 1. Motivated by

preliminary quantum chemical investigations, transient absorption spectra for 2-(2′-hydroxyphenyl)benzothiazole (HBT) were measured in the gas phase for the first time and compared to existing results in cyclohexane. As a very important result it was observed that the internal conversion in gas phase takes place in only 2.6 ps while in solution it takes about 40 times longer. Moreover, the gas phase transient signal showed a damped, low-frequency oscillation superimposed to the exponential decay, a surprising finding which needed explanation as well.

Extended static quantum chemical calculations (MR-CISD, CASSCF, RI-CC2, and TD-DFT) were performed to characterize the stationary points in the ground and in the first excited state, as well as to investigate the relaxed torsional potential. Within the limitations of each method, all of them consistently show a flat but barrierless path starting at the relaxed planar excited state geometry (keto isomer) and leading down into the direction of large torsional angles where a conical intersection between ground and first excited state was expected. MR-CISD and CASSCF calculations allowed explicit verification of the conical intersection occurring at the twisted pyramidalized geometry.

Excited-state dynamics simulations were performed at the TD-DFT level. The results show a general trend of reduction of the S_1–S_0 energy gap due to the torsional motion in the first 500 fs. The torsional motion occurs simultaneously to the pyramidalization. Between 400 fs and 500 fs, the multireference character of the wavefunction starts to become important and it is not possible to continue the simulations due to failures in the TD-DFT method. Nevertheless, the comparison between the S_1–S_0 energy gaps predicted by the dynamics simulations and by the potential energy curves confirms that HBT follows the relaxed torsional path into the direction of large torsional angles where the IC rate is very efficient. However, it should be noted that HBT need not move directly into the conical intersection as would be expected from a purely one-dimensional model. More possibly, it moves into a region of small energy gaps where the IC rate is relatively high. Therefore, the experimentally observed value of 2.6 ps fits well into the general picture given by the present dynamics simulations even though concrete calculated life times cannot be given. The strong low-frequency (40 cm^{-1}) damped oscillations superimposed to the exponential decay could be tentatively explained by the dependence of the intensity changes of the stimulated emission due to the torsional motion.

After the internal conversion at the twisted structure, HBT splits into two populations, keto and *trans*-keto. While the first one immediately isomerizes to the enol form closing the proton transfer cycle, the latter requires about 100 ps to do so. This very large difference for completing the proton transfer cycles due a very clear branching event makes HBT especially interesting for control studies.

In summary, we think we have provided a good example for a fruitful cooperation between theory and experiment leading to insights not amenable to separate investigations.

Acknowledgements

This work was supported by the Austrian Science Fund within the framework of the Special Research Program F16 (Advanced Light Sources) and Project P18411-N19. The calculations were partially performed at the Linux PC cluster Schrödinger III of the computer center of the University of Vienna. Financial support by the DFG-Cluster of Excellence: Munich-Centre for Advanced Photonics is gratefully acknowledged.

References

1 P. F. Barbara, L. E. Brus and P. M. Rentzepis, *J. Am. Chem. Soc.*, 1980, **102**, 5631–5635.
2 F. Laermer, T. Elsaesser and W. Kaiser, *Chem. Phys. Lett.*, 1988, **148**, 119–124.
3 T. Arthen-Engeland, T. Bultmann, N. P. Ernsting, M. A. Rodriguez and W. Thiel, *Chem. Phys.*, 1992, **163**, 43–53.
4 A. L. Sobolewski and W. Domcke, *Chem. Phys. Lett.*, 1993, **211**, 82–87.
5 A. Douhal, *Acc. Chem. Res.*, 2004, **37**, 349–355.
6 A. J. A. Aquino, H. Lischka and C. Hättig, *J. Phys. Chem. A*, 2005, **109**, 3201–3208.
7 S. Lochbrunner, C. Schriever and E. Riedle, in *Hydrogen-Transfer Reactions*, ed. J. T. Hynes, J. P. Klinman, H.-H. Limbach and R. L. Schowen, Wiley-VCH, Weinheim, Germany, 2006, pp. 349–375.
8 A. L. Sobolewski, W. Domcke and C. Hättig, *J. Phys. Chem. A*, 2006, **110**, 6301–6306.
9 K. Stock, T. Bizjak and S. Lochbrunner, *Chem. Phys. Lett.*, 2002, **354**, 409–416.
10 S. Lochbrunner, A. J. Wurzer and E. Riedle, *J. Phys. Chem. A*, 2003, **107**, 10580–10590.
11 S. Takeuchi and T. Tahara, *J. Phys. Chem. A*, 2005, **109**, 10199–10207.
12 C. Schriever, M. Barbatti, K. Stock, A. J. A. Aquino, D. Tunega, S. Lochbrunner, E. Riedle, R. de Vivie-Riedle and H. Lischka, *Chem. Phys.*, 2008, **347**, 446–461.
13 K. Stock, C. Schriever, S. Lochbrunner and E. Riedle, *Chem. Phys.*, 2008, **349**, 197–203.
14 C. Chudoba, S. Lutgen, T. Jentzsch, E. Riedle, M. Woerner and T. Elsaesser, *Chem. Phys. Lett.*, 1995, **240**, 35–41.
15 D. LeGourriérec, V. A. Kharlanov, R. G. Brown and W. Rettig, *J. Photochem. Photobiol., A*, 2000, **130**, 101–111.
16 T. Elsaesser and W. Kaiser, *Chem. Phys. Lett.*, 1986, **128**, 231–237.
17 R. de Vivie-Riedle, V. De Waele, L. Kurtz and E. Riedle, *J. Phys. Chem. A*, 2003, **107**, 10591–10599.
18 M. Barbatti, J. Paier and H. Lischka, *J. Chem. Phys.*, 2004, **121**, 11614–11624.
19 J. Quenneville and T. J. Martínez, *J. Phys. Chem. A*, 2003, **107**, 829–837.
20 K. Ishii, S. Takeuchi and T. Tahara, *Chem. Phys. Lett.*, 2004, **398**, 400–406.
21 T. Fujino, S. Y. Arzhantsev and T. Tahara, *J. Phys. Chem. A*, 2001, **105**, 8123–8129.
22 J. Michl and V. Bonačić-Koutecký, *Electronic Aspects of Organic Photochemistry*, Wiley-Interscience, 1990.
23 M. Barbatti, M. Ruckenbauer, J. J. Szymczak, A. J. A. Aquino and H. Lischka, *Phys. Chem. Chem. Phys.*, 2008, **10**, 482.
24 A. Migani, M. A. Robb and M. Olivucci, *J. Am. Chem. Soc.*, 2003, **125**, 2804–2808.
25 M. Barbatti, A. J. A. Aquino and H. Lischka, *Mol. Phys.*, 2006, **104**, 1053–1060.
26 M. Ben-Nun and T. J. Martínez, *Chem. Phys.*, 2000, **259**, 237–248.
27 C. A. S. Potter, R. G. Brown, F. Vollmer and W. Rettig, *J. Chem. Soc., Faraday Trans.*, 1994, **90**, 59–67.
28 A. L. Sobolewski and W. G. Domcke, *J. Phys. Chem. A*, 2007, **111**, 11725–11735.
29 G. W.-S. Y. Nosenko, M. Kunitski, I. Petkova, A. Singh, W. J Buma, R. P Thummel, B. Brutschy and J. Waluk, *Angew. Chem.*, 2008, **120**, 6126–6129.
30 C. Schriever, S. Lochbrunner, E. Riedle and D. J. Nesbitt, *Rev. Sci. Instrum.*, 2008, **79**, 013107.
31 W. C. Swope, H. C. Andersen, P. H. Berens and K. R. Wilson, *J. Chem. Phys.*, 1982, **76**, 637–649.

32 R. Bauernschmitt and R. Ahlrichs, *Chem. Phys. Lett.*, 1996, **256**, 454–464.
33 R. Bauernschmitt, M. Haser, O. Treutler and R. Ahlrichs, *Chem. Phys. Lett.*, 1997, **264**, 573–578.
34 F. Furche and R. Ahlrichs, *J. Chem. Phys.*, 2002, **117**, 7433–7447.
35 A. D. Becke, *J. Chem. Phys.*, 1993, **98**, 5648–5652.
36 O. Christiansen, H. Koch and P. Jorgensen, *Chem. Phys. Lett.*, 1995, **243**, 409–418.
37 C. Hättig, *J. Chem. Phys.*, 2003, **118**, 7751–7761.
38 A. Köhn and C. Hättig, *J. Chem. Phys.*, 2003, **119**, 5021–5036.
39 A. Schafer, H. Horn and R. Ahlrichs, *J. Chem. Phys.*, 1992, **97**, 2571–2577.
40 M. Barbatti, G. Granucci, M. Persico, M. Ruckenbauer, M. Vazdar, M. Eckert-Maksic and H. Lischka, *J. Photochem. Photobiol., A*, 2007, **190**, 228.
41 J. A. Pople, R. Seeger and R. Krishnan, *Int. J. Quantum Chem.*, 1977, **S 11**, 149–163.
42 P. J. Bruna, S. D. Peyerimhoff and R. J. Buenker, *Chem. Phys. Lett.*, 1980, **72**, 278–284.
43 R. Shepard, in *Modern Electronic Structure Theory*, ed. D. R. Yarkony, World Scientific, Singapore, 1995, vol. 1, p. 345.
44 W. J. Hehre, R. Ditchfield and J. A. Pople, *J. Chem. Phys.*, 1972, **56**, 2257–2261.
45 J. S. Binkley, J. A. Pople and W. J. Hehre, *J. Am. Chem. Soc.*, 1980, **102**, 939–947.
46 J. J. Szymczak, M. Barbatti and H. Lischka, *J. Chem. Theory Comput.*, 2008.
47 R. Shepard, H. Lischka, P. G. Szalay, T. Kovar and M. Ernzerhof, *J. Chem. Phys.*, 1992, **96**, 2085–2098.
48 H. Lischka, M. Dallos and R. Shepard, *Mol. Phys.*, 2002, **100**, 1647–1658.
49 H. Lischka, M. Dallos, P. G. Szalay, D. R. Yarkony and R. Shepard, *J. Chem. Phys.*, 2004, **120**, 7322–7329.
50 M. Dallos, H. Lischka, R. Shepard, D. R. Yarkony and P. G. Szalay, *J. Chem. Phys.*, 2004, **120**, 7330–7339.
51 H. Lischka, R. Shepard, F. B. Brown and I. Shavitt, *Int. J. Quantum Chem.*, 1981, **S.15**, 91–100.
52 H. Lischka, R. Shepard, I. Shavitt, R. M. Pitzer, M. Dallos, T. Mueller, P. G. Szalay, F. B. Brown, R. Ahlrichs, H. J. Boehm, A. Chang, D. C. Comeau, R. Gdanitz, H. Dachsel, C. Ehrhardt, M. Ernzerhof, P. Hoechtl, S. Irle, G. Kedziora, T. Kovar, V. Parasuk, M. J. M. Pepper, P. Scharf, H. Schiffer, M. Schindler, M. Schueler, M. Seth, E. A. Stahlberg, J.-G. Zhao, S. Yabushita, Z. Zhang, M. Barbatti, S. Matsika, M. Schuurmann, D. R. Yarkony, S. R. Brozell, E. V. Beck and J.-P. Blaudeau, *COLUMBUS, an ab initio electronic structure program*, release 5.9.1, 2006, www.univie.ac.at/columbus.
53 H. Lischka, R. Shepard, R. M. Pitzer, I. Shavitt, M. Dallos, T. Müller, P. G. Szalay, M. Seth, G. S. Kedziora, S. Yabushita and Z. Y. Zhang, *Phys. Chem. Chem. Phys.*, 2001, **3**, 664–673.
54 M. Barbatti, G. Granucci, H. Lischka, M. Ruckenbauer and M. Persico, *NEWTON-X: a package for Newtonian dynamics close to the crossing seam, version 0.13b*, 2007, www.univie.ac.at/newtonx.
55 F. Furche and R. Ahlrichs, *J. Chem. Phys.*, 2002, **117**, 7433–7447.
56 R. Ahlrichs, M. Bär, M. Häser, H. Horn and C. Kölmel, *Chem. Phys. Lett.*, 1989, **162**, 165–169.
57 E. Riedle, M. Beutter, S. Lochbrunner, J. Piel, S. Schenkl, S. Sporlein and W. Zinth, *Appl. Phys. B*, 2000, **71**, 457–465.
58 I. Z. Kozma, P. Baum, S. Lochbrunner and E. Riedle, *Opt. Express*, 2003, **11**, 3110–3115.
59 W. E. Brewer, M. L. Martínez and P. T. Chou, *J. Phys. Chem.*, 1990, **94**, 1915–1918.
60 S. Lochbrunner, T. Schultz, M. Schmitt, J. P. Shaffer, M. Z. Zgierski and A. Stolow, *J. Chem. Phys.*, 2001, **114**, 2519–2522.
61 S. R. Vázquez, M. C. R. Rodríguez, M. Mosquera and F. Rodríguez-Prieto, *J. Phys. Chem. A*, 2007, **111**, 1814–1826.
62 M. Moriyama, M. Kosuge, S. Tobita and H. Shizuka, *Chem. Phys.*, 2000, **253**, 91–103.
63 M. Wanko, M. Hoffmann, P. Strodet, A. Koslowski, W. Thiel, F. Neese, T. Frauenheim and M. Elstner, *J. Phys. Chem. B*, 2005, **109**, 3606–3615.
64 A. Dreuw, J. L. Weisman and M. Head-Gordon, *J. Chem. Phys.*, 2003, **119**, 2943–2946.
65 R. C. Hilborn, *Am. J. Phys.*, 1982, **50**, 982–986.
66 T. Müller, M. Dallos and H. Lischka, *J. Chem. Phys.*, 1999, **110**, 7176–7184.
67 P. G. Szalay, A. Karpfen and H. Lischka, *Chem. Phys.*, 1989, **130**, 219–228.
68 M. Dallos and H. Lischka, *Theor. Chem. Acc.*, 2004, **112**, 16–26.
69 G. Fogarasi, X. F. Zhou, P. W. Taylor and P. Pulay, *J. Am. Chem. Soc.*, 1992, **114**, 8191–8201.
70 G. Zechmann, M. Barbatti, H. Lischka, J. Pittner and V. Bonačić-Koutecký, *Chem. Phys. Lett.*, 2006, **418**, 377–382.
71 M. Barbatti and H. Lischka, *J. Am. Chem. Soc.*, 2008, **130**, 6831–6839.
72 M. Barbatti and H. Lischka, *J. Phys. Chem. A*, 2007, **111**, 2852–2858.
73 M. Barbatti, A. J. A. Aquino and H. Lischka, *Chem. Phys.*, 2008, **349**, 278–286.
74 S. Lochbrunner, A. J. Wurzer and E. Riedle, *J. Chem. Phys.*, 2000, **112**, 10699–10702.